FINAL MUON IONIZATION COOLING CHANNEL USING QUADRUPOLE DOUBLETS FOR STRONG FOCUSING

J. G. Acosta, L. M. Cremaldi, T. L. Hart, S. J. Oliveros, and D. J. Summers
University of Mississippi - Oxford, University, MS 38677 USA
D. V. Neuffer
Fermilab, Batavia, IL 60510 USA

Abstract

Considerable progress has been made in the design of muon ionization cooling for a collider. A 6D normalized emittance of $\epsilon_{6D} = 0.123\,\mathrm{mm}^3$ has been achieved in simulation, almost a factor of a million in cooling. However, the 6D emittance required by a high luminosity muon collider is $\epsilon_{6D} = 0.044\,\mathrm{mm}^3$. We explore a final cooling channel composed of quadrupole doublets limited to 14 Tesla. Flat beams formed by a skew quadrupole triplet are used. The low β^* regions, as low as 5 mm, produced by the strong focusing quadrupoles are occupied by dense, low Z absorbers that cool the beam. Work is in progress to keep muons with different path lengths in phase with the RF located between cells and to modestly enlarge quadrupole admittance. Calculations and individual cell simulations indicate that the final cooling needed may be possible. Full simulations are in progress. After cooling, emittance exchange in vacuum reduces the transverse emittance to 25 μm and lets the ϵ_L grow to 70 mm as needed by a collider. Septa slice a bunch into 17 parts. RF deflector cavities, as used in CLIC tests, form a 3.7 m long bunch train. Snap bunch coalescence combines the 17 bunches into one in a 21 GeV ring in 55 microseconds.

INTRODUCTION

The muon collider [1] offers several advantages, as compared to hadron colliders [2], to explore rare and massive events at the energy frontier due to the point like behavior of muons. It allows a relatively small collider ring. But, muons have to be cooled quickly and efficiently due to the short muon lifetime. Ionization cooling is the best cooling technique for muons and is being tested at the MICE [3] experiment. The equations describing the transverse and longitudinal cooling are given by [4]:

$$\frac{d\epsilon_\perp}{ds} = -\frac{g_t}{\beta^2}\frac{dE_\mu}{ds}\frac{\epsilon_\perp}{E_\mu} + \frac{1}{\beta^3}\frac{\beta^*_\perp}{2}\frac{(13.6\,\mathrm{MeV})^2}{E_\mu m_\mu c^2 L_R} \quad (1)$$

$$\frac{d\epsilon_L}{ds} = \frac{-\mathrm{g}_L}{\beta^2 E_\mu}\frac{dE_\mu}{ds}\epsilon_L + \frac{\gamma^3\beta_L}{\beta c^2 p^2}\pi(r_e m_e c^2)^2 n_e(2-\beta^2) \quad (2)$$

where dE_μ/ds is the energy lost calculated by the Bethe-Bloch equation. $\beta^*_\perp$ and β_L are transverse and longitudinal betatron functions. g_L and g_t are partition numbers that depend on the absorber geometry. $\epsilon_{\perp,eq}$ and $\epsilon_{L,eq}$ are the equilibrium emittances which are calculated as:

$$\epsilon_{\perp,eq} \simeq \frac{\beta^*_\perp (13.6MeV)^2}{2g_t\beta m_\mu c^2 L_R\,(dE/ds)} \quad (3)$$

$$\epsilon_{L,eq} \simeq \frac{\beta_L m_e c^2 \beta\gamma^2(2-\beta^2)}{4g_L m_\mu c^2\left[\ln\left[\frac{2m_e c^2\gamma^2\beta^2}{I(Z)}\right] - \beta^2\right]} \quad (4)$$

The transverse betatron function at the absorber should be small in order to keep the equilibrium emittance low and to reduce the heating due to multiple scattering. Strong focusing is required to cool the beam. Emittance evolution is estimated using the cooling characteristic equation 5, where i = x, y, z [4].

$$\epsilon_i(s) = (\epsilon_{0,i} - \epsilon_{i,equi})\exp(-s\frac{g_i(dP_\mu/ds)}{P_\mu}) + \epsilon_{i,equi} \quad (5)$$

Two muon cooling channels [5, 6] using the transverse cooling principle and emittance exchange have been simulated. Both show a large ϵ_{6D} reduction, but not quite enough for a muon collider as noted in Table 1.

Table 1: Helical and Rectilinear Cooling Channel normalized 6D emittances ϵ_{6D} from simulations and the emittance needed for a muon collider. The channels cool by over five orders of magnitude and need less than a factor of 10 more for a collider. The 21 bunches present after initial phase rotation are also merged into one bunch during cooling.

	ϵ_x mm	ϵ_y mm	ϵ_y mm	ϵ_{6D} mm^3
Initial Emittance [6]	48.6	48.6	17.0	40,200
Helical Cooling [5]	0.523	0.523	1.54	0.421
Rectilinear Cooling [6]	0.28	0.28	1.57	0.123
Muon Collider [7]	0.025	0.025	70	0.044

CHANNEL DESIGN

Channel Cell

According to equation 3, low equilibrium emittance requires low $\beta^*_\perp$. Strong quadrupole focusing [8] can achieve $\beta^*_\perp$ values within the required 0.5 to 2.0 cm range. A half cell is composed of two quadrupole magnets separated by a short drift space to avoid excessive fringe field interference [9] between magnets, as shown in Fig. 1 and 2. The bore diameter and length for the first quadrupole magnet

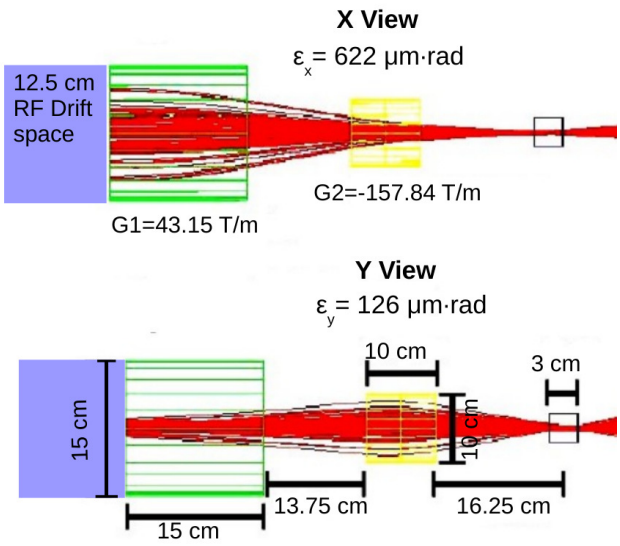

Figure 1: Half cell dimensions. RF occupies 12.5 cm on the left giving a total half cell length of 67.5 cm.

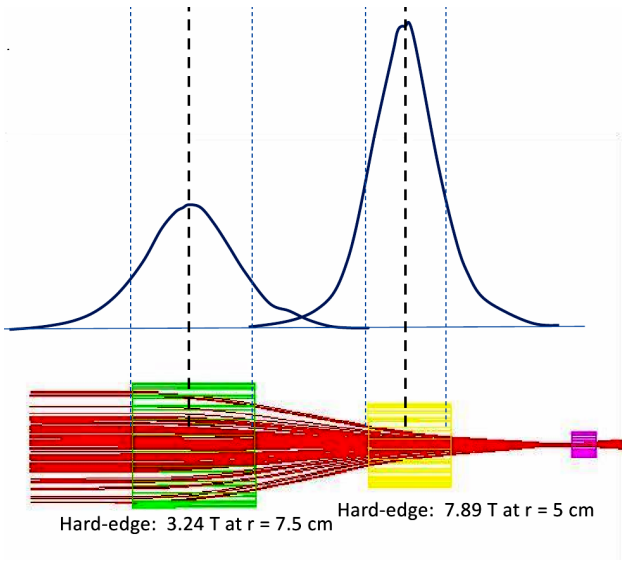

Figure 2: The fringe fields of quadrupoles [9] into each other are small. The bore diameters and lengths for the square green and yellow quadrupoles are 15 and 10 cm, respectively. The gap between quadrupoles is 13.75 cm. Quadrupole fields decrease as the cube of distance.

(Q1) is 15 cm. The bore diameter and length for the second quadrupole (Q2) is 10 cm. This configuration provides strong focusing using magnetic pole tip fields of Q1 = 3.24 T and Q2 = 7.89 T. Quadrupoles with peak fields of more than 12 T have been built with Nb_3Sn [10]. The betatron function evolution for the half cell is shown in Fig. 3.

The chosen quadrupole doublet configuration works with a flat beam near 600 MeV/c to make β_x^* and β_y^* have a 2.0 cm minimum located at the flat, 3 cm long lithium hydride absorber. As noted in Fig. 3, β^* is only small over a limited distance. So the absorber must be dense and short [12].

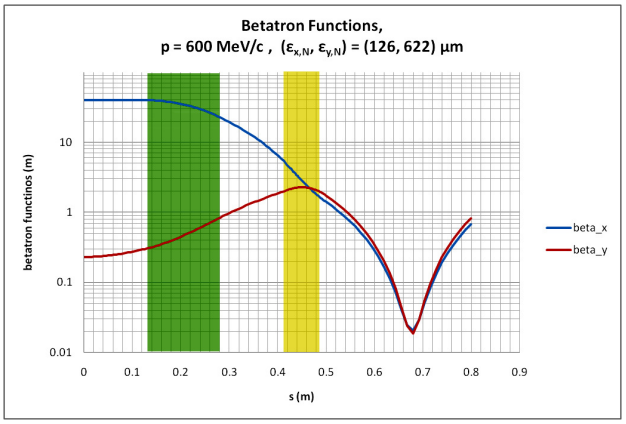

Figure 3: Half cell betatron function vs. distance s. The Courant-Snyder [11] parameters evolution through the cell is calculated using a hard edge matrix approximation and 600 MeV/c muons.

The incoming round beam has to be transformed into a flat beam. Simulations show that a round spinning, muon beam with angular momentum can be transformed into a flat non-spinning beam with a skew quadrupole triplet [13]. Cooling channels [5, 6] can impart angular momentum to a beam, but it may not be smooth enough. Alternatively and at the cost of some heating, wedges might lower x emittance and raise z emittance and then lower z emittance and raise y emittance [14].

The full cell is composed by two half cells and radio frequency cavities to recovery the longitudinal momentum lost in the absorbers. The 650 MHz radio frequency cavities are 0.125 m long, have a phase of 54.7° with respect to rising zero crossing, and a gradient of 26 MV/m. When two consecutive cells are added there are two RF cavities to recover the momentum lost. To evaluate the cell stability the trace from the transport R matrix is taken. The x and y momentum band passes overlap between 598 and 658 MeV/c. Adding another quadrupole at the absorber may be worth exploring.

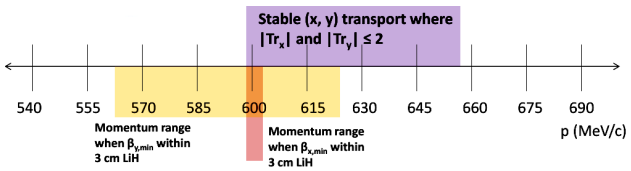

Figure 4: The cell R matrix has $|Tr(R)| < 2$ for stable transport between 598 and 658 MeV/c.

Momentum variations affect the locations for β_x^* and β_y^* as Fig. 4 shows, and can shift the minimums out of the absorbers. This effect is more visible in the x dimension for which the channel has a very narrow acceptable momentum range. To correct the $\beta_\perp^*$ shifts, sextupoles and bending magnets are being tested with a half cell to try to correct the chromaticity [15]. Bending magnets will also be needed

for emittance exchange when wedge shaped absorbers are added to the simulations.

Sextupole Addition

Introducing a bending magnet before each cell creates dispersion that with the addition of a sextupole before Q2 correct the focus shift for beams with momenta of 570 and 630 MeV/c. Figure 5 shows a bichromatic beam that has two momenta and the correction effect made by a sextupole.

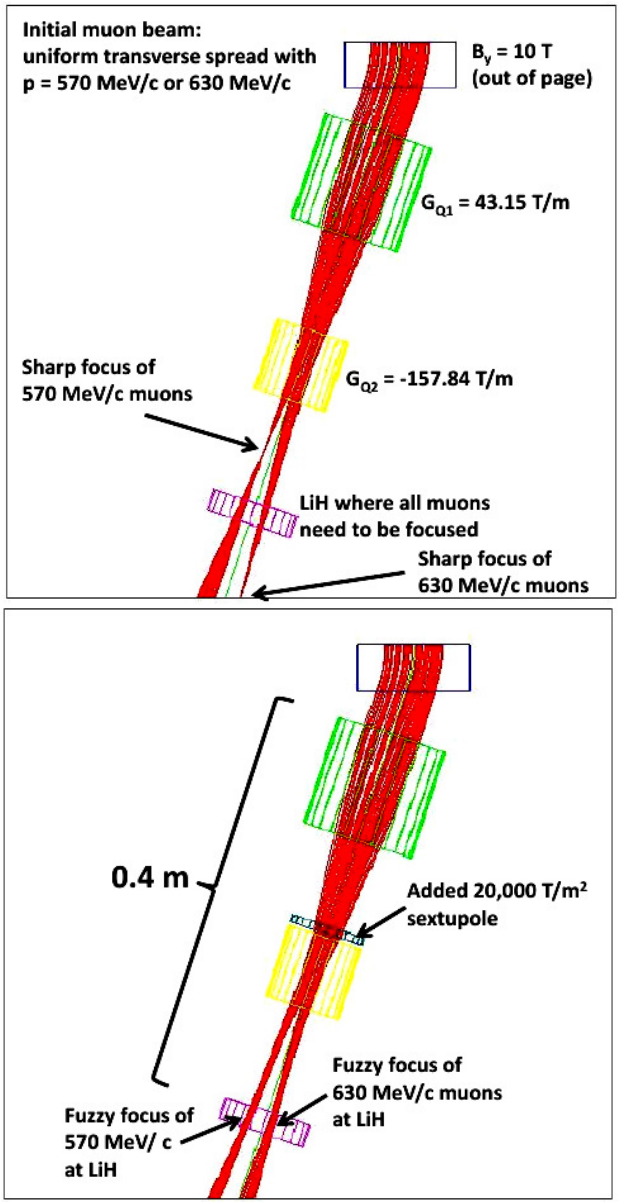

Figure 5: Half Cell with a bending magnet and sextupole to test chromaticity correction.

The sextupole shifts the focus location moving it into the absorber, but the fuzzy foci need to be fixed. This channel chromaticity correction study is in progress and not yet concluded. One possibility is to make space and put a combined function quadrupole/dipole between the RF cavities and to turn each of the two original quadrupoles into combined function quadrupole/sextupole magnets [16] by adding cos (3θ) windings.

Channel Stages

Calculations [17], but not simulations, have been done for more channel stages to complete the 6D cooling.

The low $\beta^*_\perp$ regions are occupied by absorbers made with different low Z materials such as lithium hydride, beryllium, and diamond. Table 2 shows why diamond is being considered. In spite of the equilibrium emittance increment of a factor of two from LiH to Diamond, density increases by a factor of four. Thus, the absorber thickness can be less with the same energy loss. And if β^* is reduced enough, the desired cooling can still occur.

Table 2: Material Properties for 600 MeV/c Muons [18]

Material	**Density** g/cm^3	**L_R** cm	**dE/ds** MeV/cm	**$\epsilon_{\perp,eq}$** (mm · rad)
H_2 gas	8.4×10^{-5}	7.5×10^{5}	3.522×10^{-4}	0.037
LiH	0.82	97	1.665	0.061
Be	1.85	35.3	3.164	0.087
B_4C	2.52	19.9	4.469	0.112
Diamond	3.52	12.1	6.670	0.122

To optimize the channel length, several stages with different material absorbers are required. The expected emittance evolution through the channel is plotted in Fig. 6 for 800 MeV/c muons. ϵ_{6D} is calculated using equation 5 and β^* declines from 2.0 to 0.55 cm. Each channel stage length is optimized in order to keep the total length as short as is possible. Nevertheless, cell lengths are long because a lot of RF was put in to keep β_L and the longitudinal emittance small. Shorter cell lengths may be possible.

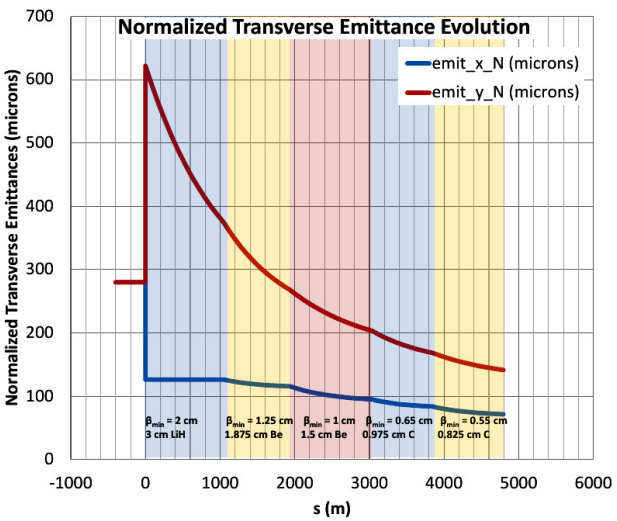

Figure 6: Expected emittance evolution [17].

Emittance exchange wedges might be placed between channel stages to optimize to flatness of the beam. Wedges might lower x emittance and raise z emittance and then lower

z emittance and raise y emittance [14]. Cooling is faster if the transverse emittance is larger.

FIRST STAGE SIMULATION

The first stage of the channel is simulated using G4beamline [19] and ICOOL [20]. The simulation runs 1000 622 ± 2 MeV/c muons through 210 cells and gets 99% muon transmission with no RF or absorber, just quadrupoles. A beam plot for the last two cells is shown in Fig. 7.

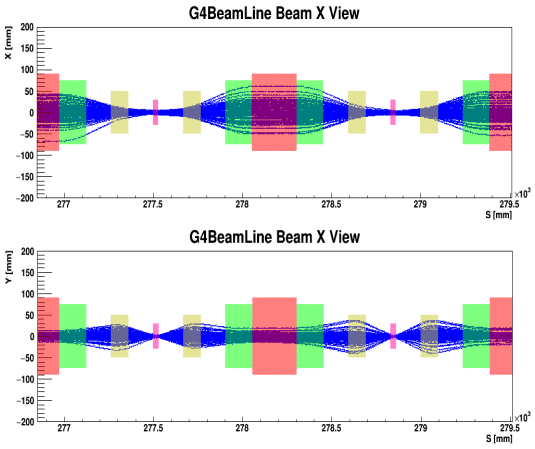

Figure 7: Last two cells for a beam emittance ϵ_x =126 μm rad and ϵ_y = 622 μm rad through 210 cells with p = 622 ± 2 MeV/c. Red is RF. Green and yellow are quadrupoles.

When absorbers and RF are included, but the stochastic process are off, the transmission drops to 50%. Finally, the transmission is 20 % when straggling and delta rays, but not scattering or decays, are activated as Fig. 8 shows.

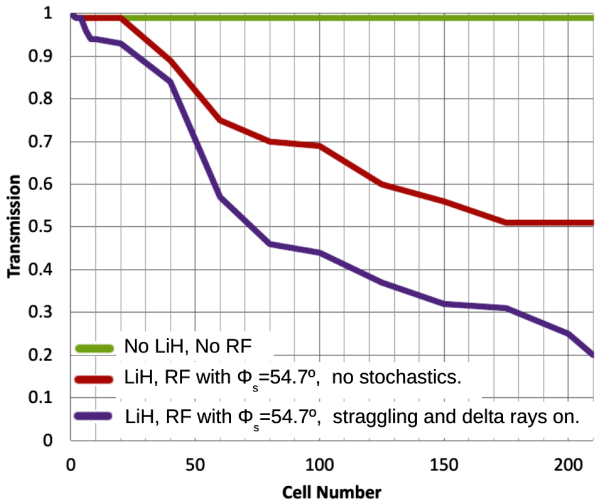

Figure 8: Transmission for a channel with 210 1.35 m cells.

The first channel stage was simulated using ICOOL and G4Beamline with p = 622 ± 2 MeV/c. Initial emittance was $\epsilon_{x,y,z}$ = (0.126, 0.622, 0.0) mm rad. Momentum shifts caused by synchrotron oscillations and perhaps different path lengths as Fig. 9 shows, mandate the addition of sextupoles.

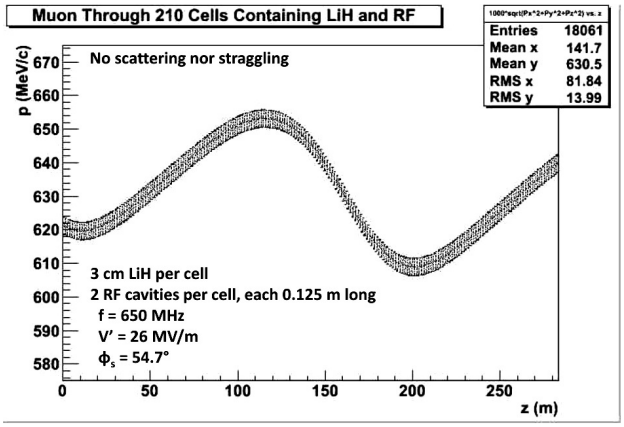

Figure 9: Longitudinal momentum oscillation for one muon through a channel with absorbers and RF.

EMITTANCE EXCHANGE

The transverse cooling is limited by the equilibrium emittance that requires very high magnetic field and dense materials to reduce the transverse emittance even modestly. Therefore, the emittance exchange proposed in [17] is placed at the end of the last cooling stage. It converts the emittance from $\epsilon_{x,y,z}$ = (0.0714, 0.141, 2.418) mm-rad to a narrower, longer $\epsilon_{x,y,z}$ = (0.025, 0.025, 70) mm-rad emittance. Fig. 10 shows a simplified illustration of the process.

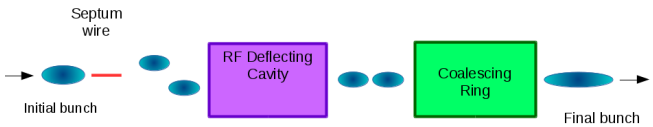

Figure 10: Emittance exchange system schema.

The system includes 16 electrostatic septa that slice the bunch into 17 parts. The Fermilab Fixed Target Switchyard used eight electrostatic septa strings to deliver beam to nine primary slow spill users and one fast spill user [21]. The bunches are interleaved into a 3.7 m long bunch train using CLIC RF deflector cavities [22]. After that snap bunch coalescense [23] combines 17 muon bunches into a single long bunch with RF in a 21 GeV ring [24,25]. The coalescing time during a quarter synchrotron period is 55 μs and the muon decay loss is 13%. The packing fraction approaches 87% [26].

CONCLUSION

The quadrupole doublet channel shows some transmission through the first stage. The transmission needs to be improved by adding magnetic sextupoles for chromatic correction. Admittance needs be moderately improved. If chromatic correction can be made to work, the channel has the potential to reduce the 6D emittance to the level needed for a high luminosity muon collider.

REFERENCES

[1] J. Gallardo et al., Snowmass 1996, BNL -52503;
D. Neuffer and R. Palmer, Conf.Proc. C940627 (1994) 52;
R. Palmer et al., Nucl. Phys. Proc. Suppl. **51A** (1996) 61;
D. Cline and D. Neuffer, AIP Conf. Proc. **68** (1980) 856;
D. Neuffer, eConf C801002 (1980) 199;
D. Neuffer, IEEE Trans. Nucl. Sci. **28** (1981) 2034;
S. Ozaki et al., BNL-52623 (2001);
D. Adey et al., Phys. Rev. **D80** (2014) 071301;
D. Neuffer, CERN-YELLOW-99 -12;
Andrew M. Sessler, Phys. Today **51N3** (1998) 48;
C. M. Ankenbrandt et al., PRSTAB **2** (1999) 081001;
M. M. Alsharo'a et al., PRSTAB **6** (2003) 081001;
R. Palmer et al., PRSTAB **8** (2005) 061003;
D. J. Summers et al., PAC 2007, arXiv:0707.0302;
D. J. Summers et al., IPAC 2012, arXiv:1207.6730;
G. T. Lyons, Master's Thesis, arXiv:1112.1105;
J. Gallardo and M. Zisman, AIP Conf. Proc. **122** (2010) 308;
Y. Alexahin et al., arXiv:1307.6129;
C. Rubbia, arXiv:1308.6612;
E. Eichten and A. Martin, Phys. Lett. **B728** (2014) 125;
V. Barger et al., Phys. Rev. **D88** (2014) 115003;
N. Chakrabarty et al., Phys. Rev. **D91** (2015) 015008;
M.-H. Wang, Y. Nosochkov, Y. Cai, and M. Palmer, IPAC-2015-TUPTY081.

[2] Michael Benedikt, Daniel Schulte, and Frank Zimmermann, Phys. Rev. ST Accel. Beams **18** (2015) 101002;
J. Tang et al., arXiv:1507.03224;
D. J. Summers et al., AIP Conf. Proc. **1507** (2012) 860;
S. J. Oliveros et al., COOL-2015-TUPF01.

[3] M. Bogomilov et al., JINST **7** (2012) P05009;
D. Adams et al., Eur. Phys. J. **C73** (2013) 2582;
D. Adams et al., arXiv:1510.08306;
L. Cremaldi et al., IEEE Trans. Nucl. Sci. **56** (2009) 1475;
D. A. Sanders, arXiv:0910.1322;
D. Adams et al., *Pion contamination in the MICE muon beam.*

[4] D. Neuffer, arXiv:1312.1266.

[5] C. Yoshikawa et al., IPAC-2014 -TUPME016.

[6] D. Stratakis and R. Palmer, PRSTAB **18** (2015) 031003.

[7] R. B. Palmer et al., PAC 2007, arXiv:0711.4275.

[8] S. Feher and J. Strait, Snowmass -1996-ACC042;
M. Berz et al., AIP Conf. Proc. **721** (2004) 413.

[9] C. Johnstone, M. Berz, D. Errede, and K. Makino, Fig. 5 on page 479, Nucl. Instrum. Meth. **A519** (2004) 472.

[10] F. Borgnolutti et al., IEEE Trans. Appl. Supercond. **24** (2014) 4003005; P. Ferracin et al., IEEE Trans. Appl. Supercond. **24** (2014) 4002306.

[11] E. D. Courant and H. S. Snyder, Annals Phys. **3** (1958) 1.

[12] D. Neuffer, Part. Accel. **14** (1983) 75.

[13] D. J. Summers et al., arXiv:1504.03972.

[14] D. Neuffer, AIP Conf. Proc., **441** (1998) 270;
D. Neuffer et al., COOL-2015-MOPF01;
D. Neuffer et al., to be published in JINST.

[15] P. Raimondi and A. Seryi, Phys. Rev.Lett. **86** (2001) 2779.

[16] V. N. Litvinenko et al., Conf.Proc. C950501 (1996) 796.

[17] D. Summers et al., IPAC 2015, arXiv:1505.01832.

[18] http://pdg.lbl.gov/2014/AtomicNuclearProperties/ ;
K. A. Olive et al., Chin. Phys. **C38** (2014) 090001.

[19] T. J. Roberts *et al.,* Conf. Proc. C0806233 (2008) WEPP120.

[20] R. C. Fernow, eConf C990329 (1999) THP31;
R. C. Fernow, Conf.Proc. C0505161 (2005) 2651.

[21] R. Joshel et al., Conf.Proc. C870316 (1987) 515;
L. W. Oleksiuk et al., IEEE Trans. Nucl. Sci. **20** (1973) 428;
C. H. Rode et al., IEEE Trans. Nucl. Sci. **18** (1971) 984.

[22] M. Aicheler et al., CERN-2012-007, p. 32;
Robert Corsini et al., PRSTAB **7** (2004) 040101.

[23] G. W. Foster, FERMILAB -TM-1902 (1994);
I. Kourbanis et al., Conf. Proc. C930517 (1993) 3799;
S. Stahl and J. MacLachlan, FERMILAB -TM-1650 (1990).

[24] R. P. Johnson, C. Ankenbrandt, C. Bhat, M. Popovic, S. A. Bogacz, and Y. Derbenev, *Muon Bunch Coalescing,* PAC07-THPMN095 (2007).

[25] Alex Bogacz, *Lattices for Bunch Coalescing,* MAP-DOC-4406 (Feb 2006).

[26] Chandra Bhat, private communication, 2015.